AIAA JOURNAL
Vol. 48, No. 4, April 2010

Classifying Induced Damage in Composite Plates Using One-Class Support Vector Machines

Santanu Das*
University of California, Santa Cruz, Santa Cruz, California 95064
Aditi Chattopadhyay†
Arizona State University, Tempe, Arizona 85287
and
Ashok N. Srivastava‡
NASA Ames Research Center, Moffett Field, California 94035

DOI: 10.2514/1.37282

For many engineering and aerospace applications, detection and quantification of multiscale damage in fiber-reinforced composite structures is increasing in importance. Consequently, the development of an efficient and cost-effective diagnosis scheme that can accurately sense, characterize, and evaluate the existence of any form of damage will offer significant potential for improving the performance, reliability, and extending the operational life of these complex systems. We present an approach to characterize and classify different damage states in composite laminates by measuring the change in the signature of the resultant wave that propagates through the anisotropic media under forced excitation. The wave propagation is measured using surface-mounted piezoelectric transducers. Sensor signals collected from test specimens with various forms of induced damage are analyzed using a pattern-recognition algorithm known as the one-class support vector machines. The one-class support-vector-machine algorithm performs automatic anomaly detection and classification of damage signatures using various features from the sensor readings. The results obtained suggest that the one-class support-vector-machine algorithm, along with appropriate preprocessing techniques, can often achieve better accuracy than the popular *k*-nearest-neighbor method in detecting and classifying anomalies caused by structural defects, even when the perturbations caused in the sensor signals due to different damage states are minimal.

Nomenclature

$f(x)$	=	decision function
$K(\mathbf{x}, \mathbf{x}_j)$	=	inner product kernel
R_{ij}	=	matrix with correct classification rate
$\mathbf{w}$	=	weight vector
$w(n)$	=	random noise
x_i	=	input pattern
y_i	=	label
α_i	=	Lagrangian multipliers
ξ	=	slack variable
ρ	=	bias
τ	=	time delay
σ	=	kernel width

I. Introduction

STRUCTURAL health monitoring (SHM) comprises the key tasks of developing a diagnosis and prognosis methodology that integrates multiscale modeling with advanced sensing technology and data interrogation procedures to efficiently provide information on both damage severity through the entire structure and localized damage patterns for structural members in a complex system.

High-performance lightweight composites and other multifunctional materials are becoming increasingly popular in many engineering applications. However, composites are also associated with complex forms of damage, and reliability is a critical issue because such defects may compromise the integrity of structures and lead ultimately to structural failure. In composites, damage may nucleate when subjected to fatigue, overloading, and low- and high-velocity impact. These forms of damage not only affect the way in which the structure responds to applied loads, but may also lead to catastrophic system failure under certain environmental conditions. In general, damage detection systems with built-in diagnosis can be of the passive-sensing type or the active-sensing type with built-in diagnostics [1,2].

Recently, in situ health monitoring using piezoelectric sensors has been addressed in several publications [3–5]. A comprehensive literature review of damage detection and health monitoring methods for structural and mechanical systems was provided by Doebling et al. [6], Chang [7,8], and Diamanti et al. [9,10]. Because damage features interact with structural features, it gives rise to numerous physical phenomena as an indicator of degradation before catastrophic failure. The presence of multiscale defects in composites, coupled with the inherent anisotropy of the material, makes detection and classification of this damage a more challenging task.

The motivation of this research is to investigate the characteristics of sensor signals in composites with various forms of induced damage and to use a novel anomaly-detection algorithm, to classify the damage. The present work implements active monitoring, in which embedded or surface-mounted actuators are used to excite the structure at certain frequency bands and a distributed sensing architecture is used to sense the mechanical response and convert the mechanical energy into equivalent voltage output. The input actuation can be tuned such that the resultant wave field is in the form of guided waves, which have been proven to be useful in detecting underlying defects or discontinuities [11,12].

Received 25 February 2008; revision received 31 March 2009; accepted for publication 12 February 2009.

*University Affiliated Research Center; Associate Scientist, NASA Ames Research Center, Mail Stop 269-2, Moffett Field, CA 94035; santanu.das-1@arc.nasa.gov.

†Professor, Mechanical and Aerospace Engineering, Director, Adaptive Intelligent Materials & Systems Center; aditi@asu.edu. Fellow AIAA.

‡Team Leader, Principal Investigator, Integrated Vehicle Health Management Program Intelligent Data Understanding Group, Mail Stop 269-4; ashok.n.srivastava@nasa.gov. Member AIAA.

The rest of this paper is organized in six sections. A detailed literature review on pattern-recognition techniques has been reported in Sec. II. Section III illustrates some of the potential applications of support vector machines (SVMs) in systems health management and the scope of our current study. Section IV describes the mathematical foundation of SVMs, with some special emphasis on the unique features of one-class SVMs, followed by some details on the optimization algorithm. Section V describes some of the applications of one-class SVMs in structural diagnostics and some details of the conducted experiments. A summary of the observations and some concluding remarks are also presented in final section.

II. Data-Driven Approaches to Systems Health Management

Pattern recognition of structural defects aims to assign a certain damage pattern to one of the recommended set of damage categories. The most popular techniques in pattern recognition can be broadly categorized as a physics-based model and a data-driven model, also known as the machine-learning approach. It is self-explanatory that the former technique is based on the fundamental understanding of the physics of the system. The prior knowledge of the process is represented in terms of quantitative or qualitative functional relationships and often dictates the approach to developing such models. A good survey on various physics-based diagnostic models can be obtained in the following literature [13–15].

Data-driven approaches rely on the use of historical data sets to train the model on nominal system behavior. Under unsupervised-learning techniques, the basic assumption is that the process has adequate knowledge of the nominal behavior of the system under investigation and that any offnominal behavior will be identified. In this work, the system is trained with the features extracted from those data sets that characterize the nominal behavior of the system and are considered as observed features. When new data are fed in, any sort of deviations or mismatches from those already observed in the training data are considered to be outliers or abnormalities. There are several existing approaches for the identification of surprise events in waveforms based on unsupervised machine-learning techniques [16–19]. Bay and Schwabacher [16] and Schwabacher [17] described an unsupervised method that works on both discrete and continuous data streams. This method is based on the nearest-neighbor approach but uses a novel pruning rule to obtain near-linear-time performance. In [18], Iverson demonstrated the inductive monitoring system (IMS) method, which is well suited to analyzing continuous data streams. IMS clusters the training data into subsets with consistent system parameters and thereafter builds the knowledge of nominal behaviors based on the data obtained either directly from the system or system model.

On the other hand, supervised-learning techniques rely on having a set of examples from each category of failure signatures to characterize different failure modes of the system. It is assumed that the given patterns or signals have already been classified by a human expert into m of n categories, based on some prior knowledge. These categories correspond to individual failure modes. Then the developed model such as a neural network, SVMs, or a decision tree learns the relationship between the input patterns or signals and the failure categories. This learning amounts to the estimation of a set of parameters of the model to maximize the classification accuracy.

Traditional techniques, such as k-nearest neighbor (k-NN) [20], projection pursuit, etc., do not assume the underlying distribution from which the training data are sampled. In the k-NN technique [20], the training data consist of both the normal and abnormal attributes of the measured data. A new test sample is evaluated by calculating the distance to the training examples located close to that point, and the labels of the close neighbors determine the classification of that sample. Recently, research has also been reported on the use of the matching pursuit decomposition (MPD)-based techniques for classifying time-varying signals [21–23]. The MPD classifiers have two levels of task. At the first level, the objective is to obtain some distinctive feature components while decomposing the signals in terms of the dictionary elements that are chosen to match the time–frequency structures of the signal. At the second level, the parameters of the extracted feature components are then used to classify the signal based on some test statistics.

In [21], Varma et al. proposed an MPD-based technique to classify time-varying acoustic signals of reinforced concrete structures. In their research, the authors established the use of MPD as a pattern-recognition tool and finally computed the classification rule based on the net contribution of the correlation coefficient information for the decomposed components from each class. The performance of the proposed classifier is indeed superior for signals having unlike patterns in time–frequency domain, but shows some drop in the probability of correct classification as the time–frequency patterns become more similar. Michaels et al. [24] conducted a comparative study on the performance of feature-based-classifiers and demonstrated some applications in SHM and nondestructive evaluation, using the wave-based technique. In [24], the author adopted a differential scheme (normal–abnormal) to compute the features in the time, frequency, or joint time–frequency domain and to examine the similarity measurement using the Fisher discriminant ratio. One of the major conclusions made by the author is that the classifier performance improves significantly with multiple input feature vectors, when compared with a single input.

Among machine-learning techniques, neural-network-based techniques for data-driven structural diagnosis and prognosis problems are well studied. During the training phase, the network is presented with different patterns with their corresponding categories, and then the high-dimensional decision space is divided into regions corresponding to each category, based on the training examples. The application of neural networks for characterizing vibration data of rotating machinery and jet engines has been presented in [25–27]. The use of dynamic wavelet neural network architecture to carry out fault prognosis of defective bearings has been reported by Vachtsevanos and Wang [28]. A comprehensive literature review of the data-driven prognostics approach can be found in [29].

III. Related Research Using Support Vector Machines

An alternative approach to pattern recognition is to develop a machine-learning technique that constructs a decision boundary based on the training data set or the predefined classes and then to check the position of the given test point with respect to the reference boundary. Recently, the SVM family has drawn considerable attention in the field of fault detection and isolation in complex systems. This is because the SVM algorithm has some powerful properties, particularly when handling very high-dimensional input data sets. The details of these properties will be explained in the later sections. Some of the existing literature representing the variety of applications using SVMs can be found in [30–36]. Zheng et al. [30] addressed the issue of isolating sensor faults in electrical power systems by implementing the support vector regression algorithm that models individual sensor responses. The authors also used the difference signal of the true and the corresponding modeled observations to build the residual classifier to isolate the sensor faults. Axelberg et al. [31] addressed the use of SVMs to classify the voltage transients due to the occurrences of multiple electrical faults. He and Shi [32] introduced a combinatorial approach in which the detailed and the approximate coefficients of the vibration signals after wavelet decomposition had been used along with SVMs to monitor the working condition of pump valves. The classification of defect states of rotating machinery (ball bearings) has been investigated by Worden and Lane [33]. This work uses the Fourier-transformed information of the vibration data to construct the classifier. Zhi-qiang et al. [34] demonstrated the use of the multiclass SVMs to determine the condition of faulty gear samples. The performance of one-class-SVM classifiers with different kernel functions and the influence of varying training (data set) size have been studied by Shin et al. [35]. Yuan and Chu [36] proposed the one-to-others multiclass SVMs to perform the fault diagnosis of turbopump rotors, and the structure of the algorithm is similar to a binary tree with a two-class-SVM classifier constructed at every node. A brief summary of the

application of different pattern-recognition techniques for structural health monitoring and damage detection is well documented in [37].

The overall objective of this research is to develop an automated data-driven technique for damage signature classification, mainly in composite structures. A database is established by conducting experiments and collecting sensor data. Composite test coupons with various types of externally induced damages such as seeded delaminations, drilled holes, notches, saw cuts, etc., were manufactured and data were collected using piezoelectric sensors. When localized damage is induced in the structure, distinct feature components of scattered waves are sensed by the neighboring transducers [38]. The normal and abnormal attributes are extracted from the measured data and are further analyzed to characterize various states of the system.

In this paper, we have investigated the ability of one-class SVMs to detect wave-based signatures of defects in sensor data under various test cases. We have demonstrated that it is possible to test subsequent data sets, once the diagnostic procedure is trained with nominal sensor data, to examine the presence of features that are significantly different from normal behavior. The current research also reveals the practicality of using the delay coordinate approach [39] along with SVMs to detect and localize the anomalous patterns in real-world problems.

The SVM model is taught the dynamics of the system from a set of scalar observations, further enabling the classifier to detect any change in dynamic characteristics that have resulted due to faults that may have occurred. One of the merits of this technique is that the occurrences of the detected outliers can easily be represented as a function of time, and therefore this method is capable of addressing some of the localization issues, especially for time-series problems. The final goal is to extract and separate the signature characteristics of the sensor signals collected from samples with various types of defects. In many cases, for a given sensor, the attributes shared between two classes are very similar to each other. To handle this problem, mutual information from multiple sensors has been used to make the decision on a particular class.

Finally, it has been shown that the proposed technique can diagnose the defects correctly and effectively using feature vectors extracted by applying Gabor's spectrogram and time-embedding method directly to the sensor response, as opposed to the differential output (i.e., normal–abnormal) [24]. It has also been demonstrated that the developed analysis based on mutual information from multiple neighboring sensors is an effective way of minimizing the possibility of false classification when coupled with a selection criterion.

IV. SVM-Based Classifier

SVM is a machine-learning technique which constructs a hyperplane decision boundary such that the margin of separation between feature vectors with positive and negative labels is maximized [40]. The SVMs provide nonlinear approximations by mapping the input vectors into high-dimensional feature spaces in which a separating hyperplane is constructed, and thereafter a decision rule is established. For example, given empirical data, $\{(x_i, y_i)\}_{i=1}^{N}$ can be categorized into 2 distinct classes based on some prior knowledge. Here, x_i represents the patterns and y_i represents the corresponding labels. For a simple problem with 2 classes, the label y_i can be used as an indicator that can hold $+1$ and -1 values, depending on which side of the decision boundary the corresponding pattern lies. It is not too difficult to establish the separating hyperplane, along with the weight vectors $\mathbf{w}$ and bias ρ, which can be defined as

$$g(x) = \mathbf{w}^T\mathbf{x} + \rho \tag{1}$$

Further details of this method can be obtained in [36]. Here, the weight vector defines the direction perpendicular to the separating hyperplane and the bias term, very often termed as an offset, as the perpendicular distance of the hyperplane from the origin, as shown in Fig. 1. The shortest distance between a separating hyperplane and the closest point is termed the margin of separation. The objective of the SVMs is to find an optimal set of these parameters ($\mathbf{w}$ and ρ) such that the margin of separation is maximized. Note that maximizing the margin of separation to achieve optimal condition is equivalent to minimizing the Euclidean norm of the weight vector.

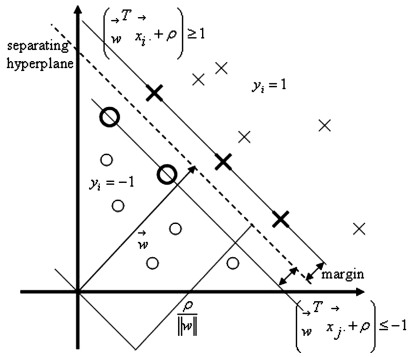

Fig. 1 Geometric representation of separating hyperplane for two-dimensional case.

A. Higher-Dimensional Mapping

As mentioned earlier, the SVMs map the n-dimensional vectors $\mathbf{w}$ of the input space X into a high- dimensional feature space in which the transformed image of the input patterns are linearly separable. This is achieved using Cover's theorem [41], which states that a multidimensional input space can be transformed to a feature space in which the transformed image of the input patterns are linearly separable, provided that the transformation is nonlinear and the dimensionality of the feature space is high enough. The high-dimensionality of the feature space enables the construction of a linear separating hyperplane in the space (Fig. 2). However, numerical optimization schemes in high dimensions would suffer from the curse of dimensionality. Such computational complexities can be avoided by taking advantage of the inner–product kernel, in which the dot product in the feature map is implicitly computed by evaluating the simple kernel, thus avoiding the explicit calculation of the feature map.

To illustrate the concept of nonlinear transformation, it has been assumed that the n-dimensional vectors $\mathbf{x}$ of the input space are mapped into an m-dimensional feature space, and the nonlinear transformation is represented by $\{\phi_j(\mathbf{x})\}_{j=1}^{m}$. With a given set of nonlinear transformation, the separating hyperplane can be expressed as

$$\sum_{j=1}^{m} w_j\phi_j(\mathbf{x}) + \rho = 0 \tag{2}$$

After some simplification and mathematical manipulation, the decision surface in the feature space can be written as

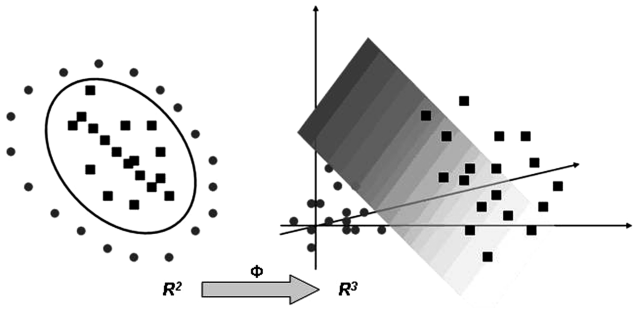

Fig. 2 Illustration of higher-dimensional mapping for linear separation fields.

$$\sum_{i=1}^{N} \alpha_i y_i \phi(\mathbf{x}_i)^T \phi(\mathbf{x}) = 0 \tag{3}$$

where $\phi(\mathbf{x}_i)^T \phi(\mathbf{x})$ represents the inner product of the two vectors in the feature space. The two vectors correspond to the input vector $\mathbf{x}$ and the ith input pattern $\mathbf{x}_i$. The inner product kernel $K(\mathbf{x}, \mathbf{x}_i)$ can be expressed as

$$K(\mathbf{x}, \mathbf{x}_i) = \sum_{j=0}^{m} \phi_j(\mathbf{x}) \phi_j(\mathbf{x}_i) \tag{4}$$

where $i = 1, 2, \ldots, N$ denotes the number of observations of the input patterns. Substituting Eq. (4) in Eq. (3), the separating hyperplane can be expressed as

$$\sum_{i=1}^{N} \alpha_i y_i K(\mathbf{x}, \mathbf{x}_i) = 0 \tag{5}$$

Because of its improved performance, the radial basis function (RBF) kernel [Eq. (6)] has been used to map the input data into an infinite-dimensional feature space. This kernel function makes use of the distances between data points, and the mapping does not depend on the position of the data set with respect to the origin. However, one key parameter is the scaling factor σ that needs to be estimated based on specific class of data set:

$$K(\mathbf{x}, \mathbf{x}_i) = \exp\left(-\frac{1}{2\sigma^2} \|\mathbf{x} - \mathbf{x}_i\|^2\right) \tag{6}$$

B. Choice of Kernel Parameter

To design the SVM classifier, it is necessary to select an appropriate kernel parameter σ for each class of data. The parameter σ controls the smoothness of the kernel function and is tuned based on the model parameter ν, such that the upper bound on the classification error is satisfied. There are several ways the parameter σ is tuned to adjust the kernel to obtain the best possible results. To obtain the optimal value of σ, the present research has adopted the method proposed by Unnthorsson et al. [42]. In this approach, for a preassigned value of ν, the SVM model is trained with a given set of data and the classification rate is plotted across a range of σ. This implies that the best possible classification accuracy that can be achieved is $1 - \nu$. The criterion for selecting the optimal σ is to obtain that value of σ for which the fraction of the correct classification rate of the training data first touches the highest classification accuracy [i.e., $(1 - \nu)\%$], as demonstrated by the straight line in Fig. 3, in which the x axis and y axis represents the σ variation and correct classification rate (in percentage), respectively. The choice of the model parameter ν is typically based on an assumption of the highest allowable fraction of misclassification of the training data. In this work, the value of ν is set to 0.05, implying that there would be 5% classification error on the training data, as shown in Fig. 3.

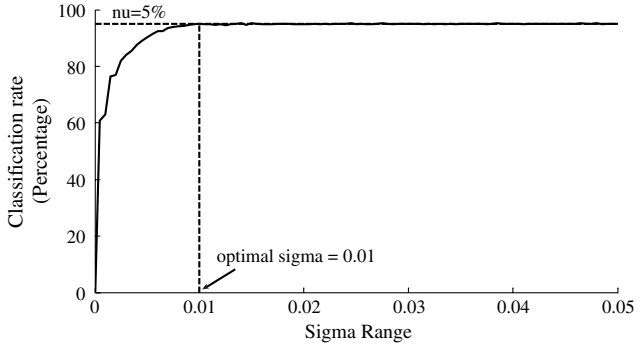

Fig. 3 Choosing the optimal value of the scale parameter sigma.

C. One-Class-SVM Algorithm

One-class SVMs belong to a unique group of the SVM family in which the training input vectors belong to one class (i.e., the class is representative of nominal system behavior). The major difference between one-class-SVM classifiers and other conventional classifiers lies mostly in how the classifiers have been trained. A one-class-SVM classifier is only trained by the reference set of a data set, and the basic assumption is that it never experienced unusual patterns or anomalous data. The separating hyperplane between two classes is constructed solely based on the training data set. Because a $(N - 1)$-dimensional hyperplane can exist in the N-dimensional feature space, the primary task is to find the optimal separating plane to maximize the margin between the origin and the hyperplane. Another important issue is to adjust the kernel width and the upper bound on the fraction of the training error such that for a given training data set, the separating hyperplane minimizes the misclassifications such as the target data rejection and acceptance of outliers. One key feature of one-class SVMs is that the majority of the training data points would lie on one side of the optimal hyperplane and any test point would be evaluated using a decision function $f(x)$ to determine which side of the hyperplane it falls on in feature space.

Figure 4 represents the schematic overview of the one-class SVM and its parameters to construct the optimal hyperplane for nonseparable patterns. This algorithm was first proposed by Schölkopf et al. [43] for estimating the support vectors of a high-dimensional distribution, and this can be achieved by solving the optimization problem as shown in Eq. (7):

$$\min_{w,\rho,\xi,b} \frac{1}{2}\mathbf{w}^T\mathbf{w} + \frac{1}{l\nu}\sum_{i=1}^{l}\xi_i - \rho \;\text{ subject to } \langle \mathbf{w}^T, \phi(\mathbf{x}) \rangle \geq \rho - \xi_i, \quad \xi_i \geq 0, \quad \text{for } \nu \in [0, 1] \tag{7}$$

where ν represents the upper bound on the fraction of the training error, ξ is the nonzero slack variable, and ρ is the offset (Fig. 4). Using Lagrangian, the constrained primal problem [Eq. (7)] is converted to a dual problem that is solved by minimizing the Lagrangian function $J(\mathbf{w}, \rho, \alpha)$ [Eq. (8)] with respect to $\mathbf{w}$ and ρ and also maximizing it with respect to Lagrange's multiplier α:

$$J(\mathbf{w}, \rho, \alpha) = \frac{1}{2}\mathbf{w}^T\mathbf{w} - \sum_{i=1}^{N} \alpha_i [y_i(\mathbf{w}^T\mathbf{x} + \rho) - 1] \tag{8}$$

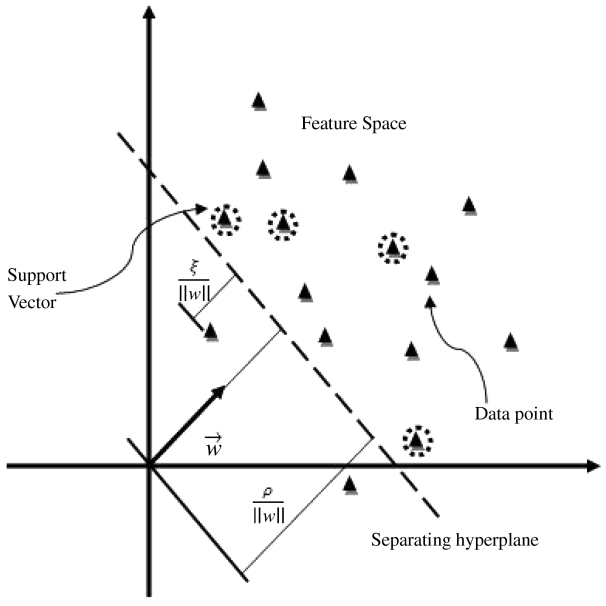

Fig. 4 Geometric interpretation of optimal hyperplane (one-class SVMs).

From the Karush–Kuhn–Tucker conditions and the two conditions of optimality, the target function in the dual problem can be written as

$$\min_{\alpha} \frac{1}{2}\sum_{i,j}\alpha_i\alpha_j K(\mathbf{x}_i,\mathbf{x}_j) \quad \text{subject to } 0 \le \alpha_i \le \frac{1}{lv}, \qquad \sum \alpha_i = 1 \tag{9}$$

The parameter ρ can be recovered for values of α_i that satisfy the given constraints in Eq. (7), and the values of $\phi(\mathbf{x}_i)$ for the corresponding nonzero α_i are termed as support vectors. The decision function for a given test vector $\phi(y)$ can be expressed as

$$f(y) = \text{sign}\left(\sum_{i=1}^{l}\alpha_i K(x_i,x_j) - \rho\right) \tag{10}$$

For the training data, the decision function takes the value of $+1$, capturing most of the data points, and -1 elsewhere. Once the dual-problem equation (9) is solved to obtain the support vectors, the optimal hyperplane is constructed in the feature space. For a new test point, the decision function evaluates which side of the hyperplane the given test point falls into, using Eq. (10). The steps of the adopted approach are shown in Algorithm 1.

Algorithm 1 One-class-SVM algorithm

1) Initialize model parameters: ν, σ (range), and training data points x.
2) For each σ, $\sigma = \sigma_{\min}, \ldots, \sigma_{\max}$.
   a) Solve the dual problem to compute α_i and ρ.
   b) Return a decision $f(x)$ on training points x.
   c) Plot the classification curve.
   d) Compute the optimal σ value.
3) Update kernel parameter σ.
4) Solve the dual problem to compute α_i and ρ.
5) Evaluate decision function $f(y)$ on test points y.
6) Output: correct classification rate and outliers.

V. Applications of One-Class SVMs

In structural health monitoring, sensor signals are analyzed to estimate and locate the severity of defects. In general, the presence of damage induces different attributes in the resulting wave propagating through the structure. In complex structures, due to additional scattering phenomena and system noise, detecting the presence of these warning transients from defective members turns out to be more complicated than anticipated. This section demonstrates the appropriateness of SVMs as a detection tool to sense different structural attributes and to identify these warning signals, depending on the system state. Throughout this research, the Ohio State University SVM classifier MATLAB Toolbox (version 3.00) has been used for the purpose of analysis.[§]

A. Detecting Unusual Patterns in Structural Data

1. Problem Description

It is an established fact that the presence of damage introduces additional nonlinearities in a medium [38]. Any type of discontinuity in the structure will give rise to different attributes, depending on the characteristics of the defect itself. Heterogeneity in the medium results in complex attenuation behaviors and thus induces distortion in the wave. The presence of damage introduces these attributes in terms of undesired attenuation, reflection components, multiple harmonics, and high-frequency burst signals. Hence, it is important that the developed diagnostics technique is sensitive to these surprising patterns. In this section, the applicability of one-class SVMs to detect unusual patterns in signals is illustrated using two test cases. Figure 5a represents a simulated sensor signal for a healthy structure. The simulated signal is a mimic of the real-life Lamb wave patterns and has been developed using attenuated and shifted versions of a basic 4.5-cycle burst signal. The presence of the damage has been represented by introducing additional attenuation, reflections, multiple harmonic components, and a high-frequency burst superimposed on the resultant wave. In addition, random noise $w(n)$ has been introduced to take into account experimental uncertainties. Here,

$$w(n) = \sqrt{V} \times \text{random}(N,1)$$

is a random variable of N realizations and variance V.

In test case 1 (Fig. 5b), the sensor response is assumed to have two additional reflection components (from a defect) when compared with the healthy response. In test case 2, the signal represents the sensor response with two additional high-frequency burst components, as shown in Fig. 5c. In both cases, two additional components are introduced at the 354th and 585th sample points. The approximate locations of those additional components have been indicated by the dotted arrow in Figs. 5b and 5c.

[§]Data available online at http://svm.sourceforge.net/download.shtml [retrieved 15 May 2009].

2. Preprocessing and Data Analysis

In wave-based methods, sensor responses are collected using a fast-data-acquisition unit that serves as the primary source of data. Depending on the nature of the transducer (piezoelectric, strain gauge, etc.), the acquired signals represent the history of the variable (voltage, strain, etc.) measured at regular intervals over time. Various input features can be obtained from the time-domain data using different preprocessing techniques, and these input features influence the performance of any data-driven algorithm. In this research, the time-embedding technique has been used to process the sensor data. The method is also known as the tapped-delay approach, in which the delay reconstruction provides the approximate dynamic information [44] of the system in terms of the scalar observations, and this is a very popular technique in the field of time-series prediction [45]. Using Taken's theorem [39], it is possible to reconstruct the attractor in the phase space from the scalar observations. Given the time observation $x(t)$, a state vector y_t can be defined as

$$y_t = [x(t), x(t-\tau), \ldots, x(t-(N_d-1)\tau)] \tag{11}$$

where the time instant $t = n/f_s$ (f_s being the sampling frequency), τ is the time delay, and N_d is the embedding dimension [45]. Further details of this technique can be found in [46].

In the current analysis, for each time history (of 2000 sample points), an 11-dimensional state vector is obtained using time delay $\tau = 1$ and embedding dimension $N = 11$. The one-class SVM is trained with these 11-dimensional input vectors from healthy samples. Then the 11-dimensional input vectors corresponding to each damaged case are tested and the corresponding labels of each data points are checked. It is observed that the majority of the unusual patterns in the signal from the defective cases have been labeled as unseen data or outliers.

Figure 6 represents the plot corresponding to the analysis corresponding to test case 1. The plots corresponding to Figs. 6a and 6b represents the resultant sensor signal from damaged structure and the reflected components introduced due to the damage, respectively. The predicted outliers are shown as peaks in Fig. 6c. Figure 7 represents a similar analysis for test case 2. In this context, it is important to note that apart from the true predictions, the outcome shows the presence of some false peaks that basically result from the presence of the random noise and the nature of the input features provided to the detection algorithm. A common practice to evaluate the performance of such a diagnostic process is to develop a confusion matrix that represents the level of agreement (or disagreement) between the true and the predicted values. The performance of the detection system to predict the presence of the additional reflection components (in test case 1) for a single realization has been evaluated with different levels of noise. The confusion matrix was constructed based on the outcome of the one-class-SVM algorithm. Figure 8 shows the trend of probability of a false alarm as a function of noise level.

Figure 9 shows a similar plot of the trend of probability of detection with different noise levels. A careful observation reveals that with increasing noise level, the probability of a false alarm tends

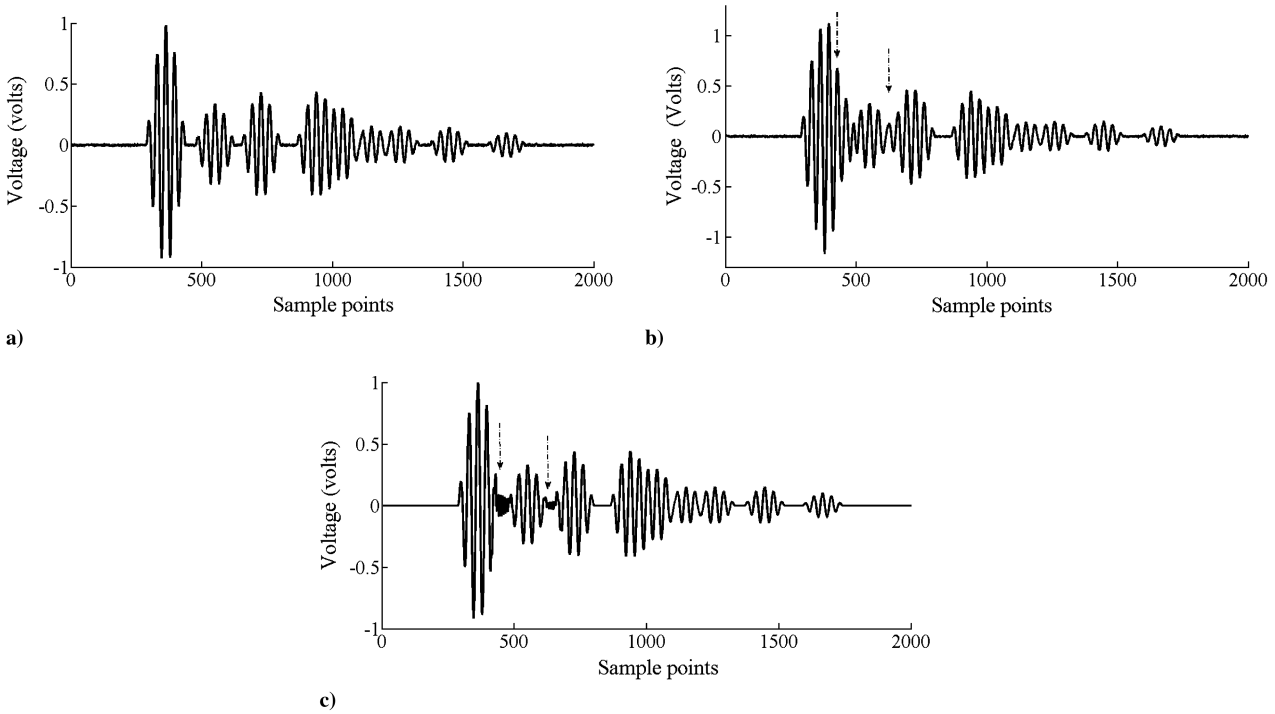

Fig. 5 Simulated sensor signals for different test cases: a) reference sensor signal, b) sensor signal with additional reflection components, and c) sensor signal with additional burst components. The locations of the additional components are shown with arrows.

to increase, whereas the probability of detection maintains a steady decay as expected. However, the sharp fall in Fig. 9 indicates that the probability of detection is heavily influenced by the increasing noise level and thus deteriorates the accuracy of the detection system.

B. Classifying Defect Patterns in Integrated Diagnostics

1. Problem Statement

In this section, the use of SVMs to investigate the changes in wave signatures in composites due to different types of damage is presented. The goal is to extract and classify the signature characteristics due to the presence of various forms of realistic defects in composite structures so that the status of the structure can be ascertained. The normal (zero state) and abnormal attributes are extracted from the measured data of a structure and are analyzed to characterize various states of the system.

2. Experimental Background

For damage quantification, experiments were conducted to obtain the response of composite plates (Fig. 10). Each plate was made up of 16 layers of carbon-fiber cyanate epoxy $[0/90]_{4s}$ laminate and was

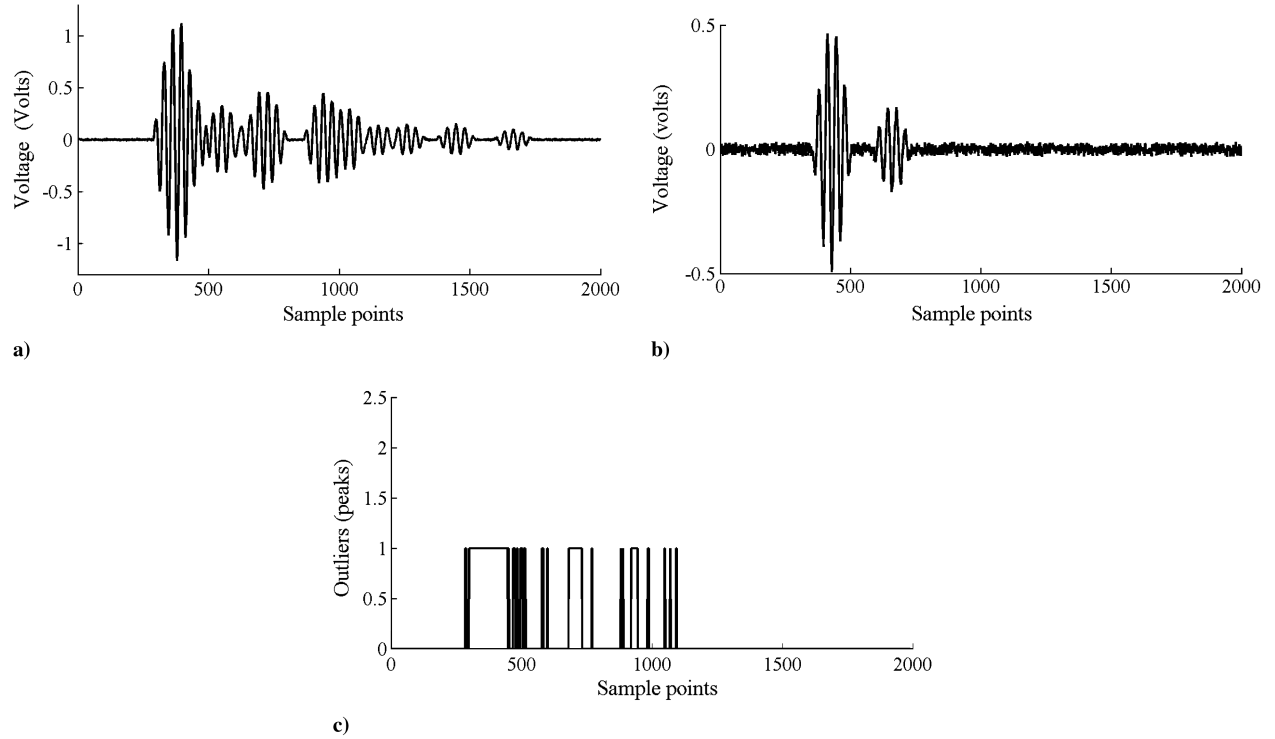

Fig. 6 Predicted outliers corresponding to additional reflections: a) simulated sensor signals with additional reflection components, b) reflection components, and c) peaks showing the presence of the outliers.

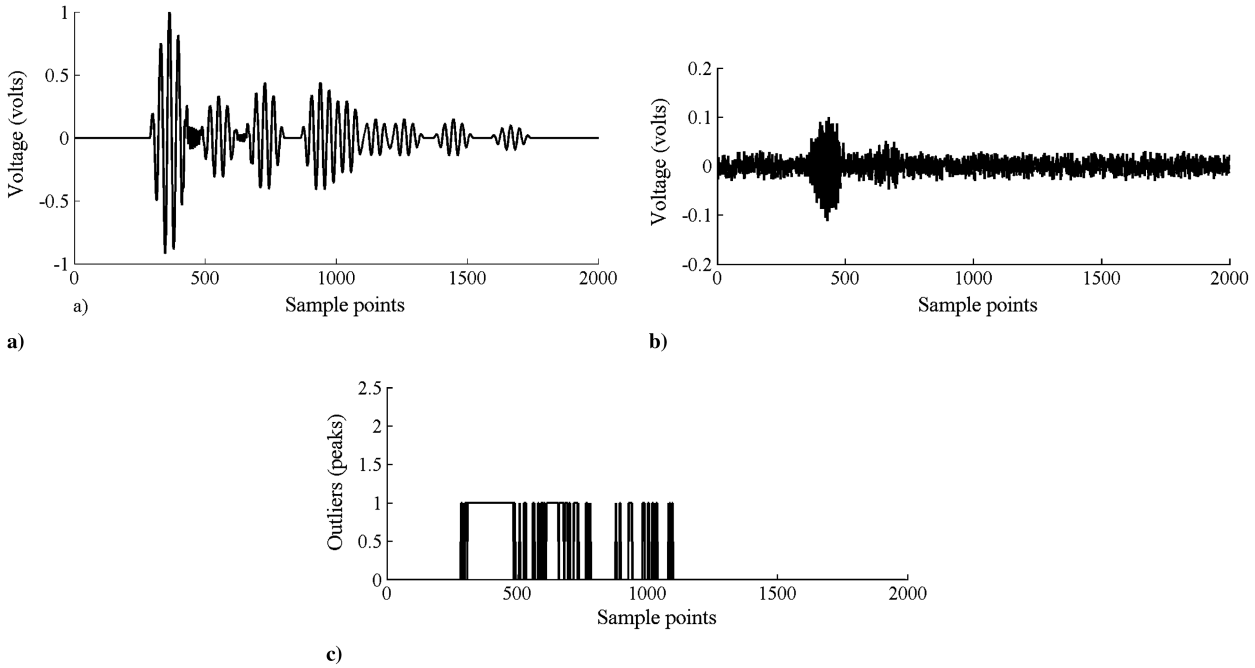

Fig. 7 Predicted outliers corresponding to high-frequency burst components: a) simulated sensor signal with additional burst components, b) burst components, and c) peaks showing the presence of the outliers.

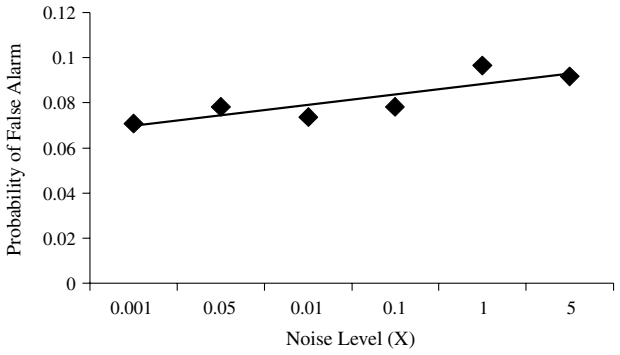

Fig. 8 Probability of false alarm vs noise level.

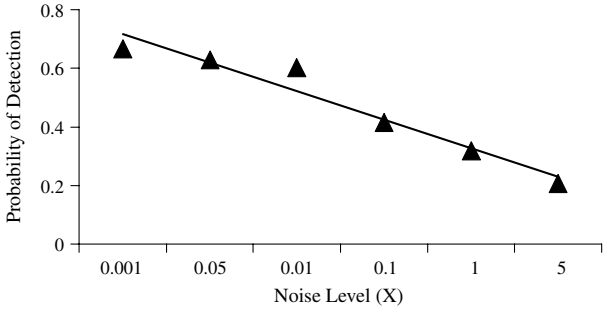

Fig. 9 Probability of detection vs noise level.

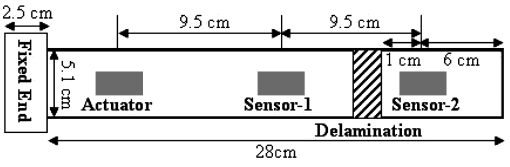

Fig. 10 Experimental setup with structural dimensions and interfaces of the composite beam.

manufactured using a hot press. The dimensions of each plate are 30.5×5.1 cm and 0.281 cm thickness. Thunder transducers (0.5×1 cm) bonded to the upper surface of the cantilever plate were used as sensors and actuators. With the actuator mounted at the clamped end, sensor 1 and sensor 2 were bonded at a distance of 9.5 and 19 cm, respectively, from the actuator (Fig. 10). To choose the excitation frequency, finite element analysis (FEA) was conducted to determine the fundamental mode shapes. The cantilevered plate ($30.5 \times 5.1 \times 0.281$ cm) was modeled in ABAQUS with 610 finite elements. The material properties used are

$$E_1 = 167 \text{ GPa} \qquad E_2 = 8.13 \text{ GPa} \qquad G_{12} = 8.8252 \text{ GPa}$$
$$G_{13} = 8.73 \text{ GPa} \qquad G_{23} = 8.73 \text{ GPa} \qquad \nu_{12} = 0.27$$
$$\nu_{21} = \left(\frac{E_2}{E_1}\right)\nu_{12} = 0.013 \tag{12}$$

Figure 11 shows the first six dominant modes for the cantilever beam with no defects. The color gradient in Fig. 11 represents the displacements profile scaled between minimum (blue) and maximum (red) values.

Table 1 shows the first six natural frequencies obtained from FEA for both healthy and damaged plates. To simulate a damage case, a 2 cm saw cut was introduced and the location of the defect was approximately 8.5 cm from the free end. From Table 1, it can be observed that natural frequencies are less sensitive to the presence of damage. Though natural frequencies and mode shapes provide

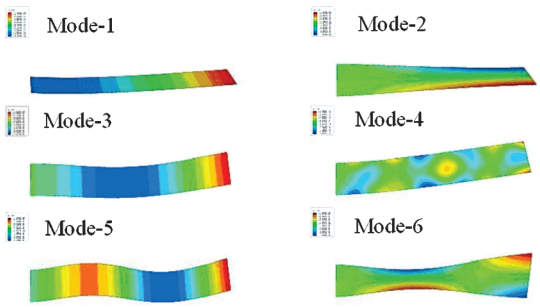

Fig. 11 Modeled mode shapes of the cantilever beam with no defect (refer to Fig. 10).

Table 1 First 6 natural frequencies of the cantilever beam with defect (saw cut) and without defect (healthy)

Modes	Frequency, Hz		
	Healthy	Damaged (saw cut)	Difference, %
1	38.895	38.996	−0.25967
2	227.84	226.75	0.478406
3	243.56	233.50	4.130399
4	612.51	604.96	1.232633
5	681.26	630.30	7.480257
6	717.87	685.72	4.478527

global information on the system, they cannot be directly used to detect the presence of the defects, because the characteristic length of the damage is much smaller than the wavelength of the excited wave. Moreover, in wave-based techniques, the choice of the actuation frequencies is important. It is critical to ensure that a fundamental mode does not get excited. This is because any excitation around the modal frequencies may result in unbounded output (displacement), as the structure may vibrate at resonance.

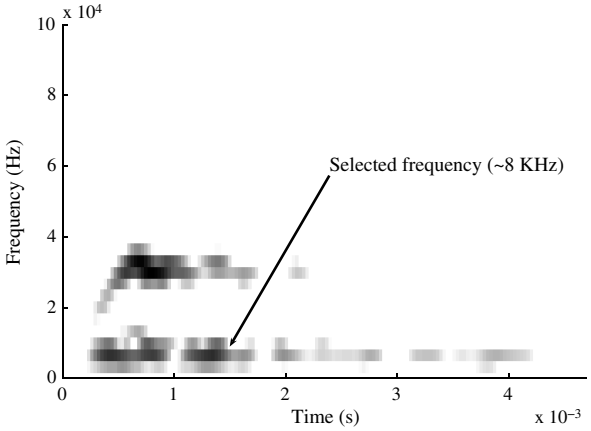

Fig. 12 Time–frequency plot of the sensor 1 response under chirp excitation.

As mentioned earlier, we have adopted an active diagnostics technique for characterizing structural defects. The piezoelectric transducer is connected to a signal generator that produces a diagnostic signal, and this results in a localized actuation in the composite laminate. The resultant wave fronts propagate through the material and are measured by the sensors. It is important to determine the frequency band(s) at which the injected actuation in the structure is maximized. This would result in an improved signal-to-noise ratio in the measured sensor response in the presence of host–structure coupling.

Experiments were conducted on healthy composite beams in which the surface-mounted actuator (Fig. 10) was excited with a 50 V peak-to-peak linear chirp signal varying from 1–100 KHz, and the subsequent responses were recorded from surface-mounted sensors 1 and 2. To observe the concentration of signal components over time, the sensor responses were represented in the time–frequency domain.

Figure 12 shows a typical time–frequency representation of the sensor 1 response using a spectrogram. Under linear chirp actuation, all frequency bands are excited with equal power. However, the frequency content of the sensor responses depends on the type of the actuator, the electromechanical coupling between the host and structure, and the transducers and the mechanical and material characteristics of the structure. In Fig. 12, two distinct frequency bands (around 8 and 32 KHz) are observed from the time–frequency plot of the sensor 1 response.

Throughout this research, a 50 V peak-to-peak 4.5-cycle tone-burst signal with a central frequency of 8 KHz was used as the excitation signal and sampled at 100 KHz. The time history of the actuation signal and the associated sensor responses for a healthy sample are shown in Fig. 13.

The investigated damages (four categories) are notches, saw cut, drilled holes, and seeded delamination introduced at the fourth interface from the midplane. The discrete delaminations have been incorporated by using 2 rectangular pieces of a Teflon sheet during the fabrication process. The other forms of defects were also introduced artificially. The dimensions of the investigated defects are

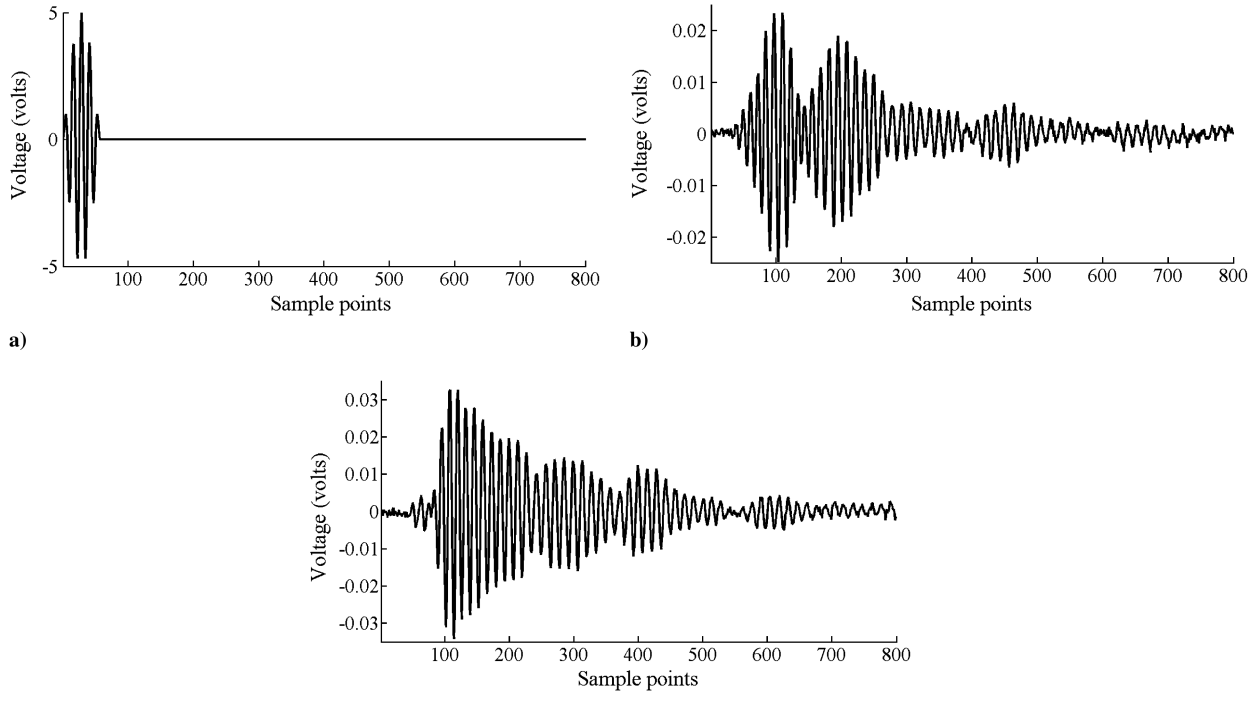

Fig. 13 Voltage history of the a) 4.5-cycle tone-burst actuator signal, b) response plots of sensor 1, and c) response plots of sensor 2 from the cantilever beam with no defect.

Table 2 Training and test class distributions for different defects on composite materials

Defect description				Training		Test	
Type	Dimension, cm	Class C	Total observations	Sets	Observations	Sets	Observations
Healthy	None	1	20	TRC1	10	TEC1	10
Delamination	4.5×5 (area)	2	20	TRC2	10	TEC2	10
Drilled holes	0.1 (diameter)	3	20	TRC3	10	TEC3	10
Notch	2.0 (width)	4	20	TRC4	10	TEC4	10
Saw cut	2.0 (length)	5	20	TRC5	10	TEC5	10

shown in Table 2. The fifth set of data belongs to the healthy group that is used as reference data for comparison. To take into account the material variability, sensor signals were collected from two identical coupons from each group. For example, four sets of measurements were conducted on a healthy specimen. A minimum of 10 observations were obtained from each transducer across each test bed under the same operating condition to take into account the experimental uncertainties associated with data acquisition. For classification, the data set consisted of 40 vectors from each sensor for each category of defects. The objective was to classify the sensor signals collected from different test beds to assist in the diagnosis of damage based on the information from the neighboring sensors (sensor 1 and sensor 2, as shown in Fig. 10).

3. *Preprocessing: Time–Frequency-Based Approach*

In the proposed scheme, the time-domain data are first downsampled by 4, and thereafter Gabor's spectrogram technique [47] (with time instants of 100, 32 frequency bins, and a Gaussian window) is used to extract the time-varying features of the sensor data for a single set from each category. Figures 14–18 represent the time–frequency structures corresponding to each category of the damaged states using spectrogram plots. Therefore, for the first set of analysis, the sensor observation is described by 100 time-localized coefficient vectors of length 32, which can be arranged into a one-dimensional feature vector of length 3200. To maximize defect information and to minimize false classification, the mutual information of the neighboring sensors is taken into account, in which each test case includes two sensors' signals (sensor 1 and sensor 2, as demonstrated in Fig. 10) and 10 observations are again obtained from each sensor to account for experimental uncertainties.

As a result, a 20-dimensional feature vector consisting of 20 one-dimensional vectors for each test bed is generated for each defect condition. Therefore, a total of 100 observations corresponding to five defect conditions (C classes) results in (3200×100)-dimensional matrices S. In the analysis, 50% of the observations

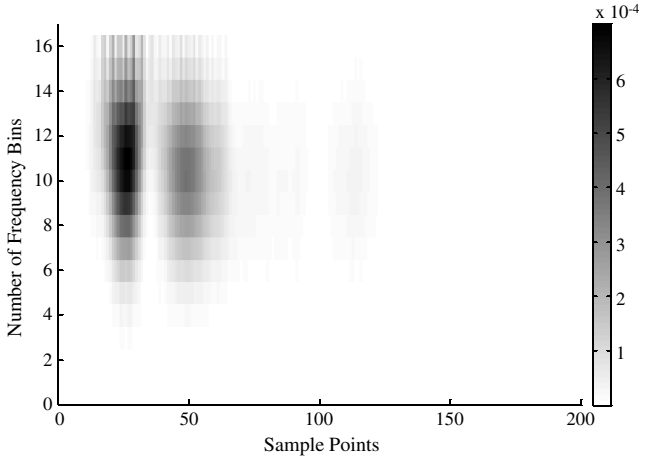

Fig. 14 Time–frequency plot of sensor 1 signal from the cantilever beam with no defect.

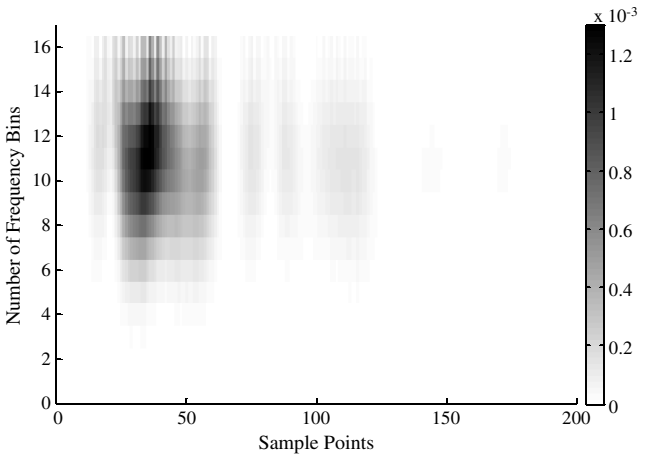

Fig. 15 Time–frequency plot of sensor 1 signal from the cantilever beam with delamination.

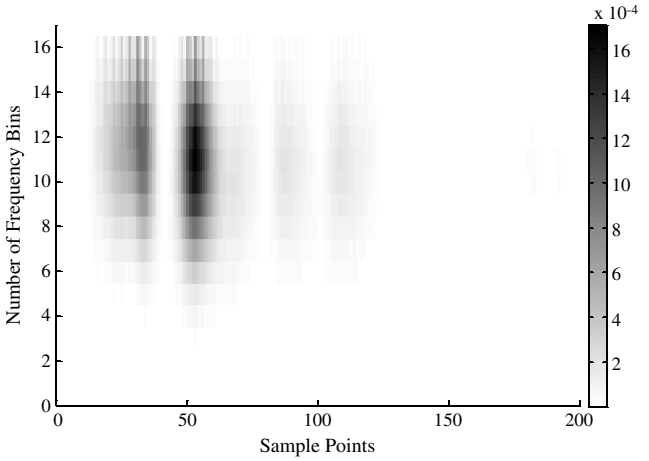

Fig. 16 Time–frequency plot of sensor 1 signal from the cantilever beam with a drilled hole.

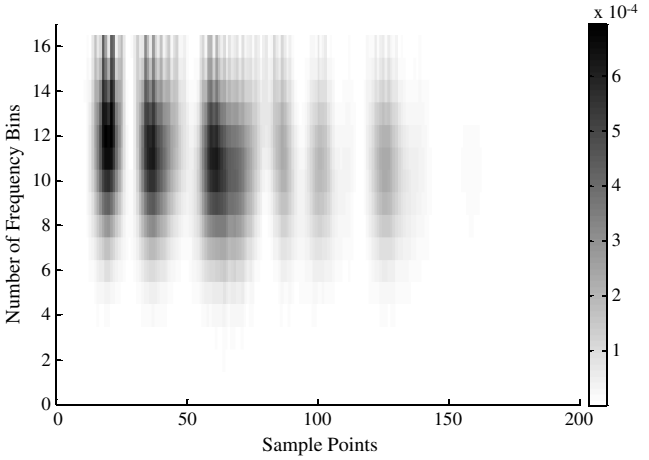

Fig. 17 Time–frequency plot of sensor 1 signal from the cantilever beam with a notch.

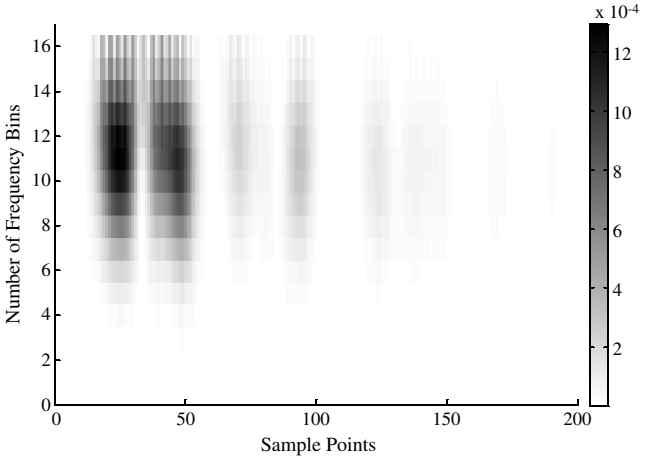

Fig. 18 Time–frequency plot of sensor 1 signal from the cantilever beam with saw cut.

related to each condition are randomly chosen and are used as training samples and the rest are used as the testing samples, as shown in Table 2.

4. Preprocessing: Time-Embedding Approach

The second set of preprocessing has been done on the same data set using the time-embedding method. The applicability of the time-embedding method along with the one-class SVMs to detect the presence of surprising features in structural data has been demonstrated in the previous sections. In this research, for each time-domain datum (of 800 sample points), an 11-dimensional state vector is obtained using $\tau = 1$ and $N = 11$. Hence, a total of (790×2200)-dimensional matrices S corresponding to five defect conditions would be available for analysis. As mentioned, 50% of the observations related to each condition are randomly chosen as the training samples and the rest are used as the test samples.

5. Selection of Appropriate Class

Table 3 presents the outcomes R using SVMs on the damage classification using an RBF kernel. Here, R_{ij} represents the correct classification rate of a data set from any jth category (representing each column) when trained with a data set from ith category (representing each row). As mentioned earlier in the one-class-SVM algorithm (Algorithm 1), for each training set and preassigned ν, the optimal σ is calculated, and thereafter the data set assigned for testing is evaluated to compute the correct classification rate. In the current analysis, ν is set to 0.05 and the optimal σ is calculated for each training set. Once the matrix R is calculated, the selection criteria that two groups of signals belong to the same class is true when R_{ij} and R_{ji} closely match with a high classification rate (i.e., $R_{ij} \cong R_{ji}$). When one-class SVMs are trained with the jth-category data set, most of the jth-category feature points lie on one side of the hyperplane, but a majority of the ith-category feature points (from the test data set) may or may not lie on the same side of the hyperplane. If features from a particular category do not lie on the same side of the hyperplane, then they are from different classes. However, if they do lie on the same side of the hyperplane, then it would be necessary to cross check if they both still lie on the same side of the hyperplane, when the SVM is trained with ith-category data set instead. The geometrical interpretation for the selection criteria means that the two hyperplanes constructed individually by ith-category and jth-category data sets have to be very similar, such that a majority of the feature points from both the categories lie on the same side irrespective of the hyperplane constructed. In the present analysis, we set the selection criteria as $\|R_{ij} - R_{ji}\| \leq 0.05(1-\gamma)$, which means that to belong to the same class, the absolute difference of the correct classification rate obtained from two sets of data must be less than or equal to 5% of the maximum classification rate.

Once the R matrix is obtained, a new matrix Q^k_{ij} is formed for the kth sensor, such that the following criteria hold:

$$\begin{aligned} &\text{If } \|R_{ij} - R_{ji}\| \leq 0.05(1-\gamma) \\ &Q^k_{ij} = Q^k_{ji} = 1 \quad \text{else} \quad Q^k_{ij} = Q^k_{ji} = 0 \end{aligned} \tag{13}$$

Table 3 Classification rate R_{ij} matrix for sensor 1 and case 1 at $\nu = 0.05$

	Test data									
Training data	TRC1	TRC2	TRC3	TRC4	TRC5	TEC1	TEC2	TEC3	TEC4	TEC5
TRC1	0.951	0.7863	0.7196	0.7210	0.6776	0.8943	0.792	0.744	0.6671	0.6663
TRC2	0.9265	0.9501	0.8260	0.8283	0.766	0.9396	0.8941	0.8535	0.7826	0.7291
TRC3	0.8950	0.8405	0.9528	0.8466	0.7425	0.9135	0.8671	0.8801	0.7780	0.7330
TRC4	0.9190	0.8746	0.8813	0.9506	0.7733	0.9255	0.9148	0.9053	0.8680	0.7661
TRC5	0.9356	0.8761	0.8745	0.8435	0.9503	0.9340	0.8940	0.8556	0.7811	0.7665
TEC1	0.8756	0.7951	0.7311	0.7181	0.6598	0.9536	0.8098	0.7406	0.6688	0.6785
TEC2	0.9166	0.8910	0.8651	0.8738	0.7845	0.9323	0.9508	0.9026	0.8205	0.7681
TEC3	0.8838	0.8160	0.8380	0.8146	0.7270	0.8886	0.8458	0.9121	0.7708	0.7101
TEC4	0.9301	0.9033	0.8875	0.9450	0.8013	0.9416	0.9290	0.9113	0.9516	0.7940
TEC5	0.9050	0.8728	0.8531	0.8393	0.7843	0.9226	0.8963	0.8618	0.8081	0.9531

Table 4 Classification rate R_{ij} matrix for sensor 2 and case 1 at $\nu = 0.05$

	Test data									
Training data	TRC1	TRC2	TRC3	TRC4	TRC5	TEC1	TEC2	TEC3	TEC4	TEC5
TRC1	0.9510	0.7863	0.7196	0.7210	0.6776	0.8943	0.7920	0.7440	0.6671	0.6663
TRC2	0.9265	0.9501	0.8260	0.8283	0.7660	0.9396	0.8941	0.8535	0.7826	0.7291
TRC3	0.8950	0.8405	0.9528	0.8466	0.7425	0.9135	0.8671	0.8801	0.7780	0.7330
TRC4	0.9190	0.8746	0.8813	0.9506	0.7733	0.9255	0.9148	0.9053	0.8680	0.7661
TRC5	0.9356	0.8761	0.8745	0.8435	0.9503	0.9340	0.8940	0.8556	0.7811	0.7665
TEC1	0.8756	0.7951	0.7311	0.7181	0.6598	0.9536	0.8098	0.7406	0.6688	0.6785
TEC2	0.9166	0.8910	0.8651	0.8738	0.7845	0.9323	0.9508	0.9026	0.8205	0.7681
TEC3	0.8838	0.8160	0.8380	0.8146	0.7270	0.8886	0.8458	0.9121	0.7708	0.7101
TEC4	0.9301	0.9033	0.8875	0.9450	0.8013	0.9416	0.9290	0.9113	0.9516	0.7940
TEC5	0.9050	0.8728	0.8531	0.8393	0.7843	0.9226	0.8963	0.8618	0.8081	0.9531

Table 5 Outcome of the classifier for case 1 at $\nu = 0.05$

	Test data									
Training data	TRC1	TRC2	TRC3	TRC4	TRC5	TEC1	TEC2	TEC3	TEC4	TEC5
TRC1	1	0	0	0	0	1	0	0	0	0
TRC2	0	1	0	0	0	0	1	0	0	0
TRC3	0	0	1	0	0	0	0	1	0	0
TRC4	0	0	0	1	0	0	0	0	0	0
TRC5	0	0	0	0	1	0	0	0	0	1
TEC1	1	0	0	0	0	1	0	0	0	0
TEC2	0	1	0	0	0	0	1	0	0	0
TEC3	0	0	1	0	0	0	0	1	0	0
TEC4	0	0	0	0	0	0	0	0	1	0
TEC5	0	0	0	0	1	0	0	0	0	1

Table 6 Classification rate R_{ij} matrix for sensor 1 and case 2 at $\nu = 0.05$

	Test data									
Training data	TRC1	TRC2	TRC3	TRC4	TRC5	TEC1	TEC2	TEC3	TEC4	TEC5
TRC1	0.9531	0.8367	0.8063	0.8012	0.7519	0.9265	0.8291	0.8038	0.7873	0.7519
TRC2	0.9696	0.9531	0.8645	0.9367	0.8341	0.9696	0.9278	0.8645	0.9417	0.8544
TRC3	0.9835	0.9341	0.9506	0.9746	0.9126	0.9810	0.9468	0.9354	0.9569	0.9189
TRC4	0.9696	0.8898	0.8645	0.9531	0.8329	0.9696	0.8860	0.8683	0.9341	0.8367
TRC5	1	0.9468	0.9354	0.9911	0.9519	1	0.9493	0.9392	0.9886	0.9227
TEC1	0.9494	0.8506	0.8316	0.8683	0.7949	0.9531	0.8417	0.8316	0.8443	0.7987
TEC2	0.9658	0.9215	0.8835	0.9506	0.8759	0.9645	0.9506	0.8810	0.9405	0.8835
TEC3	0.9974	0.9455	0.9341	0.9924	0.9227	0.9962	0.9493	0.9531	0.9860	0.9291
TEC4	0.9670	0.8797	0.8746	0.9582	0.8240	0.9632	0.8810	0.8784	0.9531	0.8291
TEC5	1	0.9569	0.9405	0.9949	0.9253	1	0.9594	0.9468	0.9949	0.9519

Table 7 Classification rate R_{ij} matrix for sensor 2 and case 2 at $\nu = 0.05$

	Test data									
Training data	TRC1	TRC2	TRC3	TRC4	TRC5	TEC1	TEC2	TEC3	TEC4	TEC5
TRC1	0.9519	0.9544	0.8873	0.9227	0.9075	0.9430	0.9557	0.8898	0.9126	0.9088
TRC2	0.8974	0.9519	0.8443	0.9050	0.8974	0.9000	0.9417	0.8519	0.8924	0.9012
TRC3	0.9670	0.9519	0.9519	0.7557	0.9075	0.9683	0.9569	0.9468	0.7189	0.9025
TRC4	0.9582	0.9873	0.8987	0.9544	0.9177	0.9607	0.9949	0.9088	0.9342	0.9113
TRC5	0.9405	0.9594	0.9569	0.9177	0.9506	0.9468	0.9594	0.9544	0.8974	0.9506
TEC1	0.9430	0.9594	0.8898	0.9265	0.9101	0.9506	0.9594	0.8924	0.9189	0.9012
TEC2	0.8126	0.9227	0.8417	0.8113	0.8746	0.8253	0.9531	0.8329	0.8025	0.8772
TEC3	0.9506	0.9354	0.9189	0.7708	0.8962	0.9443	0.9367	0.9506	0.7240	0.9000
TEC4	0.9594	0.9936	0.9050	0.9468	0.9202	0.9620	0.9987	0.9063	0.9582	0.9202
TEC5	0.9493	0.9594	0.9544	0.9215	0.9354	0.9506	0.9569	0.9594	0.9113	0.9531

Table 8 Outcome of the classifier for case 2 at $\nu = 0.05$

	Test data									
Training data	TRC1	TRC2	TRC3	TRC4	TRC5	TEC1	TEC2	TEC3	TEC4	TEC5
TRC1	1	0	0	0	0	1	0	0	0	0
TRC2	0	1	0	0	0	0	1	0	0	0
TRC3	0	0	1	0	0	0	0	1	0	0
TRC4	0	0	0	1	0	0	0	0	1	0
TRC5	0	0	0	0	1	0	0	0	0	1
TEC1	1	0	0	0	0	1	0	0	0	0
TEC2	0	1	0	0	0	0	1	0	0	0
TEC3	0	0	1	0	0	0	0	1	0	0
TEC4	0	0	0	1	0	0	0	0	1	0
TEC5	0	0	0	0	1	0	0	0	0	1

Table 9 Classification rate R_{ij} matrix for sensor 1 and case 3 at $\nu = 0.05$

	Test data									
Training data	TRC1	TRC2	TRC3	TRC4	TRC5	TEC1	TEC2	TEC3	TEC4	TEC5
TRC1	0.9544	0.9506	0.8468	0.7860	0.8202	0.9177	0.7683	0.8696	0.7911	0.8202
TRC2	0.9594	0.9506	0.8468	0.7860	0.8202	0.9177	0.7683	0.8696	0.7911	0.8202
TRC3	0.9164	0.7189	0.9506	0.6519	0.8278	0.8797	0.7012	0.8594	0.6443	0.8240
TRC4	0.8468	0.8075	0.8632	0.9531	0.8215	0.9025	0.7025	0.8455	0.6734	0.8139
TRC5	0.8797	0.6974	0.9050	0.6607	0.9557	0.8822	0.7025	0.9139	0.5962	0.9338
TEC1	0.8012	0.6506	0.8506	0.5379	0.7569	0.9544	0.6924	0.8670	0.6468	0.8278
TEC2	0.9126	0.7620	0.8670	0.7924	0.8189	0.9594	0.9531	0.8455	0.7860	0.8215
TEC3	0.9038	0.7202	0.8835	0.6835	0.8379	0.9405	0.7303	0.9519	0.6658	0.8303
TEC4	0.8822	0.6974	0.8405	0.6645	0.8025	0.8519	0.8063	0.8519	0.9544	0.8050
TEC5	0.8278	0.6873	0.9025	0.5784	0.9030	0.8721	0.6797	0.8936	0.6177	0.9544

Table 10 Classification rate R_{ij} matrix for sensor 2 and case 3 at $\nu = 0.05$

	Test data									
Training data	TRC1	TRC2	TRC3	TRC4	TRC5	TEC1	TEC2	TEC3	TEC4	TEC5
TRC1	0.9519	0.9291	0.8949	0.7936	0.9202	0.9240	0.9113	0.8949	0.8012	0.9240
TRC2	0.6658	0.9506	0.6215	0.7151	0.6683	0.8379	0.8620	0.6924	0.6582	0.6063
TRC3	0.8392	0.8645	0.9531	0.7164	0.8569	0.8341	0.8860	0.8392	0.6734	0.8506
TRC4	0.8835	0.9126	0.8075	0.9544	0.8848	0.7987	0.9075	0.7949	0.7379	0.8557
TRC5	0.8493	0.8873	0.8670	0.7367	0.9506	0.8873	0.8873	0.8746	0.7215	0.8911
TEC1	0.9177	0.9063	0.8962	0.8139	0.9240	0.9531	0.9227	0.8949	0.7974	0.9202
TEC2	0.6353	0.8594	0.6886	0.6557	0.6088	0.6594	0.9557	0.6139	0.7126	0.6645
TEC3	0.8240	0.8746	0.8341	0.6582	0.8544	0.8519	0.8670	0.9506	0.7101	0.8493
TEC4	0.8139	0.9088	0.7962	0.7582	0.8721	0.8987	0.9202	0.8215	0.9557	0.8848
TEC5	0.8417	0.8873	0.8734	0.7265	0.8911	0.8683	0.8873	0.8645	0.7341	0.9531

6. Combining Information from Sensor Pairs

For each sensor 1 ($s1$) and sensor 2 ($s2$), the Q_{ij}^{k} is evaluated and finally compared with obtain M, where

$$M = Q^{s1} \cap Q^{s2} \tag{14}$$

The matrix M represents the final outcome of the classifier based on the mutual information of the sensor pairs, and one can infer that ith-category and jth-category data sets belong to the same group if $M_{ij} = M_{ji} = 1$. Tables 3–5 represent the set of analysis results (case 1) obtained using the first set of (3200×100)-dimensional matrices with the time–frequency-based features (case 1) of the sensor data. The one-to-one-classification rate for sensor 1 and sensor 2 are given in the R_{ij} matrix in Tables 3 and 4. Table 5 represents the outcome M using Eqs. (13) and (14). Note that because the classifier is not exclusively characterizing the changes in the signature (i.e., healthy–defective), it would very often observe a majority of common attributes in a given data set, and therefore imposing selection criteria and mutual information [Eqs. (13) and (14)] from multiple sensors would minimize probable false classification. It is observed that the one-class-SVM algorithm correctly classifies classes 1, 2, 3, and 5 but is unable to categorize the notch-type defect.

The analysis results for the data set obtained from the time-embedding technique (case 2) are shown in Tables 6–8. The outcomes indicate that one-class SVMs with the time-embedded technique have better classification performance for all damaged states compared with the time–frequency-based technique. One possible explanation is the way the structural data set is presented as a result of the preprocessing using the time-embedded technique that enables one-class SVMs to separate these features in higher-dimensional space. The final set of the classification analysis was conducted for a data set collected from two identical coupons of each group (defect class) to take into account the experimental and material uncertainties associated with data acquisition and manufacturing. A minimum of 20 vectors from each sensor for each category of defects were selected from a pool of 40 vectors, and the selection was based on the two data sets having the closest distribution. In this effort, a total of (790×4400)-dimensional matrices S corresponding to 5 defect conditions were processed using the time-embedded technique. The one-class-SVM classifiers successfully classified all the defect states and are shown in Tables 9–11.

To experience the effectiveness and robustness of the adopted approach, the outcome of the one-class-SVM classifier has been compared with that of the k-nearest-neighbor algorithm with $k = 30$.

Table 11 Outcome of the classifier for case 3 at $\nu = 0.05$

	Test data									
Training data	TRC1	TRC2	TRC3	TRC4	TRC5	TEC1	TEC2	TEC3	TEC4	TEC5
TRC1	1	0	0	0	0	1	0	0	0	0
TRC2	0	1	0	0	0	0	1	0	0	0
TRC3	0	0	1	0	0	0	0	1	0	0
TRC4	0	0	0	1	0	0	0	0	1	0
TRC5	0	0	0	0	1	0	0	0	0	1
TEC1	1	0	0	0	0	1	0	0	0	0
TEC2	0	1	0	0	0	0	1	0	0	0
TEC3	0	0	1	0	0	0	0	1	0	0
TEC4	0	0	0	1	0	0	0	0	1	0
TEC5	0	0	0	0	1	0	0	0	0	1

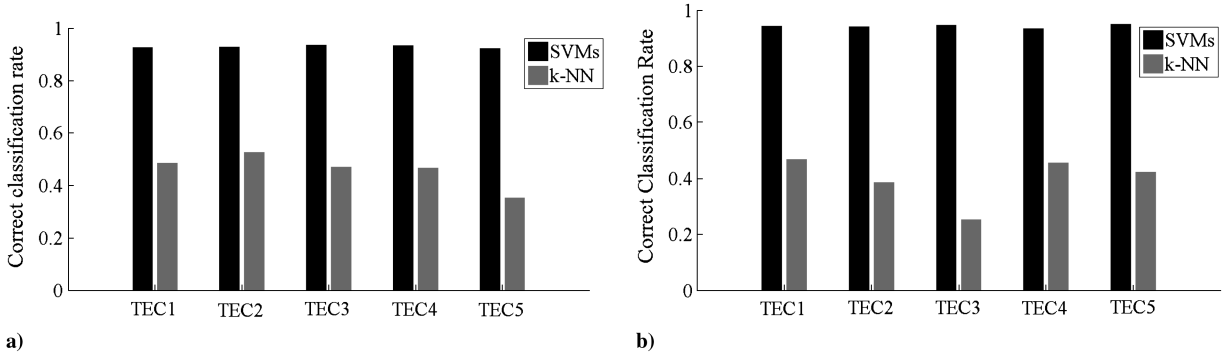

Fig. 19 Comparison of classifier performance: a) sensor 1 and b) sensor 2.

In the present study, the same data set (case 2) is preprocessed using the time-embedded method and a total of (790 × 2200)-dimensional matrices corresponding to 5 defect conditions are used for analysis purposes. The training examples comprise 50% of the observations related to each defect condition and the rest are used for validation purposes. The comparison of the performance is based on the classifier's ability to correctly classify the validation set. For example, the classifier, trained with 50% of the healthy observations, has been evaluated against the validation set of the healthy condition. Figure 19 represents a comparison of the correct classification rate for one-class-SVM and *k*-NN algorithms for different validation cases from both sensor 1 (Fig. 19a) and sensor 2 (Fig. 19b). It can be seen that the one-class-SVM-based classifier performs better than the *k*-NN on the validation set from each defect state.

VI. Conclusions

In this paper, we present a novel method based on one-class SVMs to evaluate and classify induced defects in composite laminates in terms of the changes in the signature of the resultant wave that propagates through the anisotropic medium. The ability of the one-class-SVM-based model to detect surprising patterns has been demonstrated. The paper applies the time-embedded features along with one-class SVMs to make a better detection and classification of structural defects in the presence of material and experimental uncertainties when compared with the method based on time–frequency information. Moreover, this research has shown that using multiple sensor outputs can lead to better fault characterization. In structural health management, several decomposition techniques (wavelet, matching pursuit decomposition, etc.) have been used to locate the damage using time-of-flight information. However, these decomposition techniques are computationally expensive, as they perform a component-based analysis. Application of the developed model (one-class SVMs) could be used to detect the unusual patterns, and this information could further be used to localize the presence of the outliers due to the presence of the faults, thus reducing the computational burden. Further research will be conducted to address some issues to increase the robustness of the current model in the presence of material and experimental uncertainties.

Acknowledgments

The research is supported by the U.S. Air Force Office of Scientific Research, grant number F496200310174, technical monitor Clark Allred, and NASA Ames Research Center, technical monitor Rodney Martin. Their support is gratefully acknowledged.

References

[1] Chang, F., Markmiller, J. F. C., Ihn, J., and Kok, Y. C., "A Potential Link from Damage Diagnostics to Health Prognostics of Composites Through Built-In Sensors," *Journal of Vibration and Acoustics*, Vol. 129, No. 6, 2007, pp. 718–729. doi:10.1115/1.2730530

[2] Wenger, M., Blanas P., Shuford, R. J., and Dasgupta, D. K., "Acoustic Emission Signal Detection by Ceramic/Polymer Composite Piezoelectrets Embedded in Glass-Epoxy Laminates," *Polymer Engineering and Science*, Vol. 36, 1996, pp. 2945–2954. doi:10.1002/pen.10696

[3] Tracy, M., and Roh, Y.-S., and Chang, F.-K., "Impact Damage Diagnostics for Composite Structures Using Built-in Sensors and Actuators," *Proceedings of SPIE: The International Society for Optical Engineering*, Vol. 2779, Society of Photo-Optical Instrumentation Engineers, Bellingham, WA, 1996, pp. 118–123. doi:10.1117/12.237096

[4] Staszewski, W. J., Worden, K., and Tomlinson, G. R., "Time-Frequency Analysis in Gearbox Fault Detection Using Wigner-Vile Distribution and Pattern Recognition," *Mechanical Systems and Signal Processing*, Vol. 11, No. 5, 1997, pp. 673–692. doi:10.1006/mssp.1997.0102

[5] Blanas P., Wenger, M. P., Shuford, R. J., and Das-Gupta, D. K., "Active Composite Materials and Damage Monitoring," *International Workshop on Structural Health Monitoring*, Technomic, Lancaster, PA, 1997, pp. 199–207.

[6] Doebling, S. W., Farrar, C. R., Prime, M. B., and Shevitz, D. W., "Damage Identification and Health Monitoring of Structural and Mechanical Systems from Changes in their Vibration Characteristics: A Literature Review," Los Alamos National Lab., Rept. LA-13070-MS, Los Alamos, NM, 1996.

[7] Chang, F. (ed.), *Structural Health Monitoring: Current Status and Perspectives*, Technomic, Lancaster, PA, 1997.

[8] Chang, F. (ed.), "Structural Health Monitoring," *2nd International Workshop on Structural Health Monitoring*, Technomic, Lancaster, PA, 1999.

[9] Diamanti, K., Hodgkinson, J. M., and Soutis, C. "Detection of Low-Velocity Impact Damage in Composite Plates Using Lamb Waves," *Structural Health Monitoring*, Vol. 3, No. 1, 2004, pp. 33–41. doi:10.1177/1475921704041869

[10] Diamanti, K., Soutis, C., and Hodgkinson, M. J., "Lamb Waves for the Non-Destructive Inspection of Monolithic and Sandwich Composite Beams," *Composites. Part A: Applied Science and Manufacturing*, Vol. 36, No. 2, 2005, pp. 189–195. doi:10.1016/j.compositesa.2004.06.013

[11] Guo, N., and Cawley, P., "The Interaction of Lamb Waves with Delaminations in Composite Laminates," *Journal of Acoustical Society of America*, Vol. 94, No. 4, 1993, pp. 2240–2246.

[12] Giurgiutiu, V., "Tuned Lamb Wave Excitation and Detection with Piezoelectric Wafer Active Sensors for Structural Health Monitoring," *Journal of Intelligent Material Systems and Structures*, Vol. 16, 2005, pp. 291–305. doi:10.1177/1045389X05050106

[13] Gertler, J., "A Survey of Model Based Failure Detection and Isolation in Complex Plants," *IEEE Control Systems Magazine*, Vol. 8, No. 6, 1988, pp. 3–11. doi:10.1109/37.9163

[14] Benkhedda, H., and Patton, R. J., "Fault Diagnosis Using Quantitative and Qualitative Knowledge Integration," *UKACC International Conference on Control*, Vol. 2, Inst. of Electrical and Electronics Engineers, Piscataway, NJ, 1996, pp. 849–854.

[15] Isermann, R., "Model-Based Fault-Detection and Diagnosis—Status and Applications," *Annual Reviews in Control*, Vol. 29, No. 1, 2005, pp. 71–85. doi:10.1016/j.arcontrol.2004.12.002

[16] Bay, S., and Schwabacher, M., "Mining Distance-Based Outliers in Near Linear Time with Randomization and a Simple Pruning Rule," *Proceedings of the Ninth ACM SIGKDD International Conference on Knowledge Discovery and Data Mining*, Association for Computing

Machinery, New York, 2003, pp. 29–38.
[17] Schwabacher, M., "Machine Learning for Rocket Propulsion Health Monitoring," *2005 SAE World Aerospace Congress*, Vol. 114, Society of Automotive Engineers, Warrendale, PA, 2005, pp. 1192–1197.
[18] Iverson, D. L., "Inductive System Health Monitoring," *Proceedings of the International Conference on Artificial Intelligence*, Vol. 2, CSREA Press, Las Vegas, NV, June 2004, pp. 605–611.
[19] Budalakoti, S., Srivastava, A. N., and Akella, R., "Discovering Atypical Flights in Sequences of Discrete Flight Parameters," *Proceedings of the IEEE Aerospace Conference*, Inst. of Electrical and Electronics Engineers, Piscataway, NJ, Mar. 2006, pp. 1–8.
[20] Khan, M., Ding, Q., and Perrizo, W., "*k*-Nearest Neighbor Classification on Spatial Data Streams Using P-Trees," *Proceedings of the 6th Pacific-Asia Conference on Advances in Knowledge Discovery and Data Mining*, Vol. 2336, Springer–Verlag, London, 2002, pp. 517–518.
[21] Varma, S. P., Papandreou-Suppapola, L., and Suppappola, S. B., "Detecting Faults in Structures Using Time-Frequency Techniques," *International Conference on Acoustics, Speech, and Signal Processing*, Vol. 6, IEEE Computer Society, Los Alamitos, CA, May 2001, pp. 3593–3596.
[22] Ebenezer, S. P., Papandreou-Suppappola, A., and Suppappola, S. B., "Classification of Acoustic Emissions Using Modified Matching Pursuit," *EURASIP Journal on Applied Signal Processing*, Vol. 2004, No. 3, 2004, pp. 347–357.
doi:10.1155/S1110865704311029
[23] Papandreou-Suppappola, A., and Suppappola, S. B., "Analysis and Classification of Time-Varying Signals with Multiple Time-Frequency Structures," *IEEE Signal Processing Letters*, Vol. 9, Mar. 2002, pp. 92–95.
doi:10.1109/97.995826
[24] Michaels, J., Cobb, A., and Michaels, T., "A Comparison of Feature-Based Classifiers for Ultrasonic Structural Health Monitoring," *Health Monitoring and Smart Nondestructive Evaluation of Structural and Biological Systems III*, Proceedings of SPIE, Vol. 5394, Society of Photo-Optical Instrumentation Engineers, Bellingham, WA, 2004, pp. 363–374.
[25] Samanta, B., Al-Balushi, K. R., and Al-Araimi, S. A., "Bearing Fault Detection Using Artificial Neural Networks and Genetic Algorithm," *EURASIP Journal on Applied Signal Processing*, Vol. 2003, No. 3, 2005, pp. 366–377.
doi:10.1155/S1110865704310085
[26] Brotherton, T., Jahns, J., Jacobs, J., and Wroblewski, D., "Prognosis of Faults in Gas Turbine Engines," *Proceedings of the IEEE Aerospace Conference*, Vol. 6, Inst. of Electrical and Electronics Engineers, Piscataway, NJ, 2000, pp. 163–171.
[27] Tumer, I. Y., and Huff, E. M., "Analysis of Triaxial Vibration Data for Health Monitoring of Helicopter Gearboxes," *Journal of Vibration and Acoustics*, Vol. 125, 2003, pp. 120–128.
doi:10.1115/1.1526130
[28] Vachtsevanos, G., and Wang, P., "Fault Prognosis Using Dynamic Wavelet Neural Networks," *AUTOTESTCON Proceedings IEEE Systems Readiness Technology Conference*, Inst. of Electrical and Electronics Engineers, Piscataway, NJ, 2001, pp. 857–870.
[29] Schwabacher, M., "A Survey of Data-Driven Prognostics," AIAA Infotech@Aerospace Conference, AIAA Paper 2005-7002, 2005.
[30] Zheng, S., Han, Z., Tang, H., and Zhang, Y., "Application of Support Vector Machines to Sensor Fault Diagnosis in ESP System," *Proceedings of the 2004 International Conference on Machine Learning and Cybernetics*, Vol. 6, Inst. of Electrical and Electronics Engineers, Piscataway, NJ, 2004, pp. 3334–3338.
[31] Axelberg, P. G. V., Irene G., and Bollen, M. H. J., "Support Vector Machine for Classification of Voltage Disturbances," *IEEE Transactions on Power Delivery*, Vol. 22, No. 3, 2007, pp. 1297–1303.
doi:10.1109/TPWRD.2007.900065
[32] He, F., and Shi, W., "WPT-SVMs Based Approach for Fault Detection of Valves in Reciprocating Pumps," *Proceedings of the American Control Conference*, Vol. 6, Inst. of Electrical and Electronics Engineers, Piscataway, NJ, 2002, pp. 4566–4570.
[33] Worden, K., and Lane, J. A., "Damage Identification Using Support Vector Machines," *Smart Materials and Structures*, Vol. 10, No. 3, 2001, pp. 540–547.
doi:10.1088/0964-1726/10/3/317
[34] Zhi-qiang, J., Han-guang, F., and Ling-jun, L., "Support Vector Machine for Mechanical Faults Classification," *Journal of Zhejiang University Science*, Vol. 6, No. 5, 2005, pp. 433–439.
[35] Shin, J. H., Eom, D., and Kim, S., "One-Class Support Vector Machines—An Application in Machine Fault Detection and Classification," *Computers and Industrial Engineering*, Vol. 48, No. 2, 2005, pp. 395–408.
doi:10.1016/j.cie.2005.01.009
[36] Yuan, S., and Chu, F., "Support Vector Machines-Based Fault Diagnosis for Turbo-Pump Rotor," *Mechanical Systems and Signal Processing*, Vol. 20, No. 4, 2006, pp. 939–952.
doi:10.1016/j.ymssp.2005.09.006
[37] "A Review of Structural Health Monitoring Literature: 1996-2001," Los Alamos National Lab., Rept. LA-13976-MS, Los Alamos, NM, 2003.
[38] Das S., Kyriakides, I., Chattopadhyay, A., and Papandreou-Suppappola, A., "Monte Carlo Simulation Matching Pursuit Decomposition Method for Damage Quantification in Composite Structures," *Journal of Intelligent Material Systems and Structures*, Vol. 20, No. 6, 2009, pp. 647–658.
doi:10.1177/1045389X08097386
[39] Buzug, T., and Pfister, G., "Optimal Delay Time and Embedding Dimension for Delay-Time Coordinates by Analysis of the Global Static and Local Dynamical Behavior of Strange Attractors," *Physical Review A*, Vol. 45, No. 10, 1992, pp. 7073–7084.
doi:10.1103/PhysRevA.45.7073
[40] Smola, A. J., Bartlett, P. L., Schölkopf, B., and Schuurmans, D., *Advances in Large-Margin Classifiers*, MIT Press, Cambridge, MA, 2000, Chap. 1.
[41] Taylor, S. J., and Cristianini, N., *Kernel Methods for Pattern Analysis*, Cambridge Univ. Press, Cambridge, England, U.K., 2004.
[42] Unnthorsson, R., Runarsson, R. T., and Johnson, T. M., "Model Selection in One Class nu-SVMs Using RBF Kernels," *16th Conference on Condition Monitoring and Diagnostic Engineering Management*, Växjö Univ. Press, Växjö, Sweden, Aug. 2003.
[43] Schölkopf, B., Platt, J. C., Shawe-Taylor, J., Smola, A. J., and Williamson, R. C., "Estimating the Support of a High-Dimensional Distribution," *Neural Computation*, Vol. 13, No. 7, 2001, pp. 1443–1472.
doi:10.1162/089976601750264965
[44] McSharry, E. P., "Innovations in Consistent Nonlinear Deterministic Prediction," D.Phil. Thesis, Univ. of Oxford, Oxford, 1999.
[45] Perez-Cruz, F., and Bousquet, O., "Kernel Methods and Their Potential Use in Signal Processing," *Signal Processing Magazine*, Vol. 21, No. 3, 2004, pp. 57–65.
[46] Zhang, J., and Lam, K. C., "Time Series Prediction Using Lyapunov Exponents in Embedding Phase Space," *Processing of ICSP*, Inst. of Electrical and Electronics Engineers, Piscataway, NJ, 1998, pp. 221–224.
[47] Simone, G., Morabito, F., Polikar, R., Ramuhalli, P., Udpa, L., Udpa, S., and Williamson, R. C., "Feature Extraction Techniques for Ultrasonic Signal Classification," *International Journal of Applied Electromagnetics and Mechanics*, Vol. 15, Nos. 1–4, 2002, pp. 291–294.

B. Balachandran
Associate Editor